# Pose Sensing With a Single RFID Tag

Jia Liu<sup>®</sup>, Member, IEEE, ACM, Shigang Chen<sup>®</sup>, Fellow, IEEE, Min Chen<sup>®</sup>, Member, IEEE, Qingjun Xiao, Member, IEEE, ACM, and Lijun Chen<sup>®</sup>

Abstract—Determining an object's spatial pose (including orientation and position) plays a fundamental role in a variety of applications, such as automatic assembly, indoor navigation, and robot driving. In this paper, we design a fine-grained pose sensing system called Tag-Compass that attaches a single tag to an object (whose size may be small) and identifies the tagged object's pose by determining the spatial orientation and position of the tag. We exploit the *polarization* properties of the RF waves used in the communications between an RFID reader and the tag on the object. Polarization mismatch between the tag and the reader's antenna affects the received signal strength at the reader. From the measured signal strength values, we are able to deduce the tag's pose through a series of transformations and deviation minimization. We propose a system design for Tag-Compass and implement a prototype. We evaluate the performance of Tag-Compass through extensive experiments using the prototype. The experimental results show that Tag-Compass provides accurate estimate of object orientation with a median error of just 2.5° when the tag's position is known and a median error of 3.8° when the tag's position is unknown. In the latter case, Tag-Compass will provide an estimate of tag position as a byproduct of orientation sensing, with an accuracy comparable to the state of the art. It is practically appealing to find both the orientation and the position of an object using a single method, instead of having to deploy two different methods.

Index Terms—RFID tag, orientation estimation, localization, linear polarization.

## I. INTRODUCTION

RADIO frequency identification (RFID) has wide applications in object tracking [2]–[7], supply chain management [8]–[10], and warehouse inventory [11]–[16]. The RFID

Manuscript received October 29, 2017; revised January 14, 2019, January 5, 2020, and April 5, 2020; accepted June 8, 2020; approved by IEEE/ACM Transactions on Networking Editor Y. Guan. Date of publication August 11, 2020; date of current version October 15, 2020. This work was supported in part by the National Natural Science Foundation of China under Grant 61702257 and Grant 61771236, in part by the Natural Science Foundation of Jiangsu Province under Grant BK20170648, in part by the U.S. National Science Foundation under Grant CNS-1409797 and Grant CNS-1718708, in part by the Fundamental Research Funds for the Central Universities under Grant 14380066, and in part by the Collaborative Innovation Center of Novel Software Technology and Industrialization. A preliminary version of this article appeared in the proceedings of IEEE INFOCOM'17. (Corresponding authors: Jia Liu; Lijun Chen.)

Jia Liu and Lijun Chen are with the State Key Laboratory for Novel Software Technology, Nanjing University, Nanjing 210023, China (e-mail: jialiu@nju.edu.cn; chenlj@nju.edu.cn).

Shigang Chen is with the Department of Computer and Information Science and Engineering, University of Florida, Gainesville, FL 32611 USA (e-mail: sgchen@cise.ufl.edu).

Min Chen is with Google Inc., Mountain View, CA 94043 USA (e-mail: minchen@google.com).

Qingjun Xiao is with the School of Computer Science and Engineering, Southeast University, Nanjing 211189, China (e-mail: csqjxiao@seu.edu.cn). Digital Object Identifier 10.1109/TNET.2020.3007830

tags are becoming ubiquitously available in our daily life as they make their way into retail products, library books, debit cards, passports, driver licenses, car plates, medical devices, etc. This paper studies an under-investigated problem, identifying a tagged object's spatial pose, including its orientation and position, which is equivalent to determining its tag's direction and location in space. Solving this problem has practical importance for a variety of applications. In manufacturing, products on an assembly line may need to face towards a certain direction for automated operations such as painting, labeling, or component assembling [17], [18] to be performed at the correct area or spot on each product. It is thus useful as a quality control mechanism to automatically check the correct orientation of all or a randomly-sampled subset of tagged products on an assembly line right before the point of operation. If accurate orientation measurement can be made, the small number of misaligned objects may be moved back to face the correct direction by a robotic arm or other mechanisms. In a packaging company, the ability of detecting the exact orientation of tagged objects inside each package can help provide assurance at the end of a packaging line that objects are placed correctly inside (instead of upside down, for example). In indoor navigation systems, knowing the pose of a tagged object can ensure reliable docking guidance towards the target of interest [19], [20]. In robotics, estimating the position and orientation of a tagged robot offers critical information for autonomous driving [21].

Although much advancement was achieved on RFID-based applications in recent years, the problem of determining an object's pose, particularly its orientation, has not received adequate attention. The most related work is RF-Compass [22], which is tailored to a specific application setting of robotic assembly, where a robot with several attached tags moves towards an object (e.g., a desk leg for assembly) which carries two tags. By comparing the signals from all tags, an RFID reader can roughly determine the positions of the two tags on the object through a space partitioning technique. The line segment between the two positions gives a reference about the object's orientation, based on which the robot will adjust its movement. The performance of RF-Compass relies on the localization accuracy of the two tags on the object, as well as the distance between the tags. For the general problem of determining the orientation of an object, we may remove the robot from the system and replace its coarse localization function with the most advanced localization algorithms for RFID tags, such as PinIt [3] and DAH [4]. Both of them achieve great indoor localization accuracies, with the former having a median error of 11.2cm and the latter having a median error of 12.3cm. Such accuracies would be sufficient if the tagged object is long and thus the two tags can be far apart (for example, a couple of meters apart). However, if the object is short in the dimension(s) where the tags must be placed for measuring the direction, those best localization algorithms will be inadequate. For example, if the dimensions of the object in the horizontal plane (where the direction will be measured) are  $20cm \times 20cm$ , in our experiments, they result in mean directional errors of  $30.0^{\circ}$  and  $31.6^{\circ}$ , respectively, which are too large for many applications.

This paper introduces Tag-Compass, a fine-grained pose sensing system that uses a single tag to determine the orientation as well as the position of the associated object; the single-tag solution can be applied to objects big or small, down to the size of the tag. Since even the state-of-theart localization algorithms are proven to be inadequate for orientation estimation, we resort to a completely different method based on the polarization properties of the RF waves used in the communications between an RFID reader and the tag on the object. The observation is that, as the RF waves travel from the reader to the tag and back, if the tag's direction and the polarization of the incoming wave (which is in turn determined by the reader antenna's direction) are not fully aligned, it causes polarization mismatch, thereby affecting the received signal strength (RSS) at the reader. This power loss due to polarization mismatch is referred to as polarization loss factor (PLF). With the RSS values measured by the reader, we can derive PLF and further deduce the tag's relative direction with respect to the reader antenna's direction. With the latter a known quantity, we can then figure out the tag's absolute direction in space, which in turn gives us the object's orientation (whose relationship with the tag's direction is fixed after the tag is attached to the object). However, designing such a system is not simple because the received signal power relies on various physical-layer characteristics besides PLF, such as antenna gains, radiation pattern and reflection coefficients, whose values are unknown and may vary with environmental conditions. Besides, the tag position that determines PLF is also unknown by the reader in some applications.

In this paper, we propose a system design for Tag-Compass and a computational method that separates PLF from all other physical-layer characteristics (which will then be estimated as a whole). This allows us to isolate the impact of PLF, from which we can eventually determine the tag's direction. Tag-Compass is designed to operate under two cases, with the knowledge of the tag's position or without, which have their respective applications: in the previously-discussed assembly line application, the position where each product pauses for orientation measurement is fixed and known; in the indoor navigation case, the tag's position is not pre-known. Without knowing the tag's position a priori, we exploit two metrics, RSS deviation and angle variance, to build a family of holograms, which help us find the tag's direction and also its location as a byproduct, eliminating the need of deploying a separate system for tag localization. Even though our system also needs the tag's location in its computation, we use polarization properties as our main approach for direction finding. This new approach can tolerate localization error much better than the previous non-polarization approach that simply uses two tags' locations to determine a direction. Our experiments show that Tag-Compass has a median error of just 2.5° when the tag's position is pre-known and a median

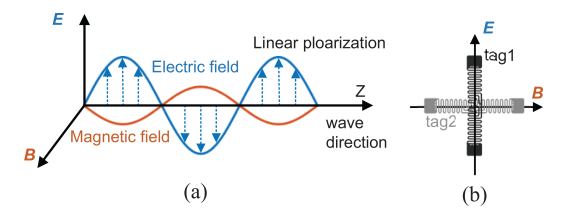


Fig. 1. (a) Linearly polarized wave, (b) relationship between the tag direction and polarization.

error of  $3.8^{\circ}$  when the tag's position is not known. Besides, the localization accuracy of Tag-Compass is comparable to the state of the art [3], [4].

The main contributions of this paper are summarized as follows: First, this work performs fine-grained direction finding based on polarization properties, using a single tag. Second, its accuracy is far better than the prior art for objects of small dimensions. Third, the proposed method can estimate the location of a tag (hence the tagged object) as a byproduct. Fourth, we implement a prototype of Tag-Compass based on the commercial off-the-shelf (COTS) tags and readers, and demonstrate its performance through extensive experiments.

## II. MOTIVATION AND BACKGROUND

## A. Polarization and Object's Orientation

Polarized waves are electromagnetic waves in which the vibrations occur in a single plane. *Polarization* indicates the direction of the electric field of a polarized wave, which is perpendicular to the propagation direction of the wave [23]. As shown in Fig. 1(a), the electromagnetic wave travels along the Z axis. The electric field is in a vertical plane (E-Z plane) and the magnetic field is in a horizontal plane (B-Z plane), which are always in phase and at 90 degrees to each other. For the linearly polarized wave, the polarization direction is along a single line (same as the direction of the electric field). This paper uses linearly polarized waves in the communications between an RFID reader and a tag to sense the spatial pose.

Most commercial tags (e.g., ALN-9640 Squiggle [24]) contain a narrow wire-like metal foil behaving like a dipole antenna: If the tag is fully aligned with the electric field of incoming wave, the electrons are pushed back and forth from one end of the tag antenna to the other, ensuring sufficient voltage to power the integrated circuit for computation and communication (tag<sub>1</sub> in Fig. 1(b)). In contrast, if the tag is directed perpendicular to the electric field, electrons move back and forth just across the tiny width of the metal foil, producing no detectable voltage and thereby failing to drive the tag (tag<sub>2</sub> in Fig. 1(b)). For other angles between the tag and the electric field, the power level produced lies between the above two cases. The closer the angle is towards full alignment, the stronger the power that the tag produces, which is measurable by the reader from the reflected signal emitted by the tag.

This paper attempts to exploit the orientation-dependent physical characteristics of tag-reader communications for the purpose of determining an object's pose, especially the orientation. We define the *direction of a tag* to be the direction from one end of the dipole to the other end; the starting end may be chosen arbitrarily. The *orientation of an object* can be conveniently defined under different application contexts.

For a product on an assembly line, we may simply use the direction of its tag as its orientation. For a robot, we may define its orientation to be the direction which its face is pointing to. In general, after a tag is fixed onto an object, its direction of placement relative to the object's orientation is fixed. Hence, at any time, if we can figure out the absolute direction of the tag in space, we will know the orientation of the object. So the problem becomes determining the tag's direction. Next, we know the polarization of the incoming wave based on the direction of the reader's antenna, a quantity that can be controlled. Our conjecture is that there should be a way by which we can find the tag's absolute direction in space based on the strength of the reflected signal received by the reader from the tag, because we know that this signal strength is functionally related to the alignment between the direction of the tag and the polarization of the incoming wave.

## B. Friis Equation

The extended Friis equation [25] provides a mathematical description of the power received by the receiver from the transmitter, as shown below.

$$P_R = P_T \frac{G_T G_R \lambda^2}{(4\pi r)^2} (1 - |\Gamma_T|^2) (1 - |\Gamma_R|^2) |\hat{\mathcal{P}}_T \cdot \hat{\mathcal{P}}_R|^2, \quad (1)$$

where  $P_R$  is the received power,  $P_T$  is the transmit power,  $\lambda$  is the wavelength, r is the distance between the transmitter and the receiver,  $G_R$  and  $G_T$  denote the angular-dependent receiver gain and transmitter gain, respectively,  $\Gamma_T$  indicates the transmitter reflection coefficient,  $\Gamma_R$  indicates the receiver reflection coefficient. Of most interest to us are  $\hat{\mathcal{P}}_T$  and  $\hat{\mathcal{P}}_R$ , which are the transmitter polarization vector and the receiver polarization vector, specifying the polarization of the electromagnetic wave from the transmitter and the direction of the receiver's antenna in space, respectively. The squared dot product  $|\hat{\mathcal{P}}_T \cdot \hat{\mathcal{P}}_R|^2$  of these two vectors is defined as the polarization loss factor (PLF).

The extended Friis equation describes the received power one way from the transmitter to the receiver. The communication between an RFID reader and a tag is a round trip, including the *uplink* from the reader to the tag, and the *downlink* by which the tag backscatters the incoming wave back to the reader [23]. Therefore, derived from (1), the received power  $P_{RX,reader}$  at the reader is:

$$\begin{cases} P_{RX,reader} = P_{TX,reader} \times C \times PLF \\ PLF = PLF \uparrow \times PLF \downarrow \\ C = \xi \times \frac{G_{reader}^2 \times G_{tag}^2 \times \lambda^4}{(4\pi r)^4} (1 - |\Gamma_{reader}|^2)^2 (1 - |\Gamma_{tag}|^2)^2, \end{cases}$$
(2)

where  $P_{TX,reader}$  is the original transmit power from the reader,  $\xi$  is the radiation efficiency that measures how well a tag converts accepted power to radiated power, C is called the *diversity* term capturing most parameters in (1) under notations in the context of reader-tag communication,  $PLF\uparrow$  is the polarization loss factor of the uplink,  $PLF\downarrow$  is the polarization loss factor of the downlink, and PLF is the product of the two. Most COTS readers, e.g., ALN-9900+ [26] and ImpinJ R420 [27], are able to measure the received power when a tag is successfully interrogated. The power is reported

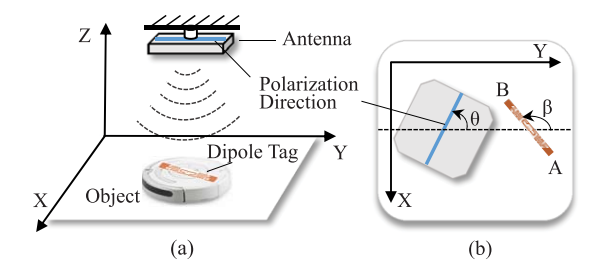


Fig. 2. (a) System deployment, (b) top view of the antenna's polarization angle  $\theta$  and the tag's orientation angle  $\beta$ .

in a logarithmic form, referred to as RSS (Received Signal Strength), as follows.

$$RSS = 10(\lg P_{TX,reader} + \lg C + \lg PLF). \tag{3}$$

With the RSS measurements, we develop Tag-Compass, which determines the tag's direction based on the polarization characteristics in tag-reader communications.

#### III. TAG-COMPASS OVERVIEW

# A. System Deployment

Tag-Compass uses any widely-available commercial dipole tag, e.g., ALN-9640 Squiggle [24], as the vehicle to determine an object's orientation. As shown in Fig. 2(a), a dipole tag residing in the horizontal x-y plane is deployed on the top of an object. The vector connecting the two endpoints of the tag from A to B is the tag's direction, denoted by  $\overrightarrow{AB}$ . As shown in Fig. 2(b), we refer to the direction angle from the y-axis to  $\overrightarrow{AB}$  as the *tag's orientation angle*, denoted by  $\beta$ ,  $0 \le \beta < 2\pi$ , which also specifies the direction of the tag. Clearly, the tag's orientation angle  $\beta$  will change by the same degrees (radians) as the tagged object changes its orientation. With a fixed angular relationship between the tag and the object, we can easily deduce the object's orientation from  $\beta$ .

Suppose the surveillance region is covered by one or a small number M of linearly polarized patch antennas (such as Larid PA9-12 [28]), denoted as  $A = \{A_1, A_2, ..., A_M\}$ , with known locations, where  $M \geq 1$ . These antennas above the region hang from the ceiling and are parallel to the horizontal plane, as shown in Fig. 2(a). They are connected to a reader. For simplicity, we use  $A_m$  to represent the mth antenna as well as its coordinates, where  $1 \le m \le M$ . Each antenna  $A_m$ is able to electronically or mechanically rotate its polarization direction, i.e., the polarization of the generated waves. We refer to the incline angle between the y-axis and the polarization direction as polarization angle, denoted by  $\theta$ , as shown in Fig. 2(b). Initially, the polarization is aligned with the y-axis, i.e.,  $\theta = 0$ . When the polarization direction is rotated in cycles from  $\theta = 0$  to  $\theta = 2\pi$ , the reader continuously schedules the antennas in round robin and collects the RSS sample measurements from the tag. For each antenna, we select a certain number N of samples, each having an RSS value and a value of  $\theta$  at which the RSS measurement is taken.

Formally, we use a matrix  $\mathcal{R} = \{r_{m,n}\}$  to depict the RSS measurements from all antennas, where  $r_{m,n}$  is the nth RSS value measured by the mth antenna,  $1 \leq m \leq M, 1 \leq n \leq N$ . We also collect the corresponding polarization angle matrix  $\Theta = \{\theta_{m,n}\}$  when each RSS value is measured, where  $\theta_{m,n}$ 

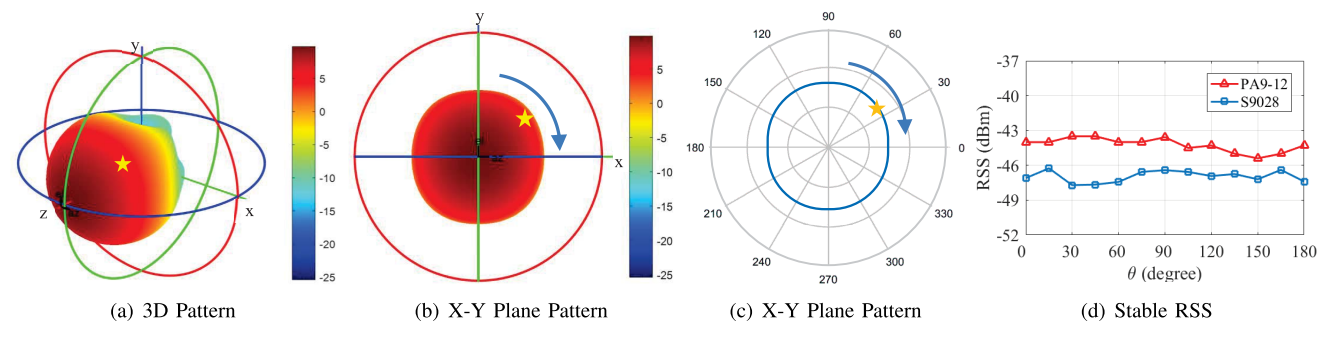


Fig. 3. The antenna gain remains largely stable as the antenna rotates.

is the polarization angle of the mth antenna when collecting the nth RSS value, i.e.,  $r_{m,n}$ . We formulate the pose sensing problem as follows: Given  $\mathcal{A}$ ,  $\mathcal{R}$ , and  $\Theta$ , how to determine the tag's orientation angle  $\beta$  and the tag position?

# B. Solution Overview

As research on localization has achieved great advancement, Tag-Compass pays more attention to estimating the tag's orientation angle  $\beta$ , which will be discussed in two cases.

- First, we consider the direction-finding problem with the priori knowledge of the tag's position, denoted as T. Such positional information can be automatically estimated through one of the numerous existing tag localization protocols [2]–[4], [6]. With this information, we will discuss how to use  $\mathcal{A}$  and  $\Theta$  to fit the measured  $\mathcal{R}$  and then derive  $\beta$ .
- Second, we remove the requirement of knowing the tag's position in advance. We propose three types of holograms to locate the tag as well as determine the tag's orientation angle.

# IV. DIRECTION FINDING WITH KNOWN TAG POSITION

# A. Rationale

The extended Friis equation (2) describes the received power by the reader. Consider a reader antenna. When we rotate its polarization direction (in the plane parallel to the x-y plane), all parameters except for the polarization loss factor almost stay unchanged. Now we validate this conclusion as follows. In Fig. 3(a), we plot a patch antenna's radiation patterns with Antenna Toolbox [29] in Matlab. Antenna Toolbox is a widely used tool that provides functions and apps for the design, analysis, and visualization of antenna elements and arrays [29]. We set the radio frequency of the antenna to 900Mhz (which is the operating frequency of the UHF RFID system) and other parameters are default. The patch antenna is placed at the origin (0,0,0) and faces to the z-axis. Fig. 3(a) shows the theoretical 3D radiation pattern. Consider a tag under the antenna's coverage, which is labelled as a star. When the patch antenna rotates counter-clockwise (view from z-axis) around z-axis in the x-y plane, it is equivalent to that the tag (star) rotates around z-axis clockwise, in the plane that is parallel to x-y plane (as shown in Fig. 3(b)). The motion trajectory forms a circle shown in Fig. 3(c). Clearly, the antenna gains  $(G_{reader})$  at these positions on the circle almost remain stable. Besides, the other parameters in the diversity term C do not change as the antenna rotates, including the radiation efficiency  $\xi$ , the antenna gain of the tag  $G_{tag}$ , the wave length  $\lambda$ , transmitter reflection coefficient  $\Gamma_{reader}$  and the

receiver reflection coefficient  $\Gamma_{tag}$ . Therefore, the received power  $P_{RX,reader}$  varies with only PLF as the polarization direction rotates.

We further validate the above theoretical conclusion with real experiments. Two kind of antennas, a linearly polarized patch antenna (Laird PA9-12 [28]) and a circularly polarized patch antenna (Laird S9028 [28]), are used in our experiments. The antenna is placed at (0, 0, 100)cm and faces to -z-axis. A tag is placed at the point (20, 20, 0)cm. To see if the received power remains stable as the antenna rotates around z-axis, we need to remove the impact of polarization loss, which means that we shall rotate the tag and the antenna by the same degrees each time. Fig. 3(d) shows the measured RSS values with respect to the rotation angles of the antennas. We can see that RSS values remain largely stable, -44dBm for PA9-12 and -47dBm for S9028, as the polarization direction changes. The slight variance is negligible compared with the large variance caused by polarization mismatch. We have repeated the above experiment many times with different tag placements and different tag orientations. The same is observed. RSS almost remains stable, suggesting that the received power is stable when the antenna rotates around z-axis, which agrees with the theoretical results. Given the measured RSS value, Tag-Compass will search the orientation angle space to find the best angle whose PLF predicts a received power from (2) that matches best with the measured

## B. Calculating PLF

Recall that the PLF in the round-trip RFID communication consists of  $PLF\uparrow$  and  $PLF\downarrow$ . Consider an arbitrary reader antenna  $A_m$ . Denote its coordinates as  $(a_x,a_y,a_z)$ . Let the tag's coordinates T be  $(t_x,t_y,t_z)$ . As shown in Fig. 2, the vector that specifies the tag's direction is:

$$t(\beta) = (-\sin\beta, \cos\beta, 0), \tag{4}$$

where  $\beta$  is the tag's orientation angle. Similarly, the polarization direction  $\boldsymbol{a}$  of the antenna at  $A_m$  is:

$$\mathbf{a}(\theta) = (-\sin\theta, \cos\theta, 0),\tag{5}$$

where  $\theta$  is the polarization angle of the antenna. For the uplink (from the antenna to the tag), the electromagnetic wave emitted by  $A_m$  travels along the vector  $\overrightarrow{A_mT}$ :

$$\overrightarrow{A_mT} = (i, j, k) = (t_x - a_x, t_y - a_y, t_z - a_z).$$
 (6)

The polarization vector  $\boldsymbol{u}(A_m,T,\theta)$  of the electromagnetic wave at the tag's position T is the projection of  $\boldsymbol{a}$  on the plane that is perpendicular to the vector  $\overrightarrow{A_mT}$  [30]. Hence, we have:

$$\mathbf{u}(A_m, T, \theta) = \frac{(u_1, u_2, u_3)}{\sqrt{u_1^2 + u_2^2 + u_3^2}},\tag{7}$$

where

$$\begin{cases} u_1 = \frac{i \times (i \times sin\theta - j \times cos\theta)}{i^2 + j^2 + k^2} - sin\theta \\ u_2 = \frac{j \times (i \times sin\theta - j \times cos\theta)}{i^2 + j^2 + k^2} + cos\theta \\ u_3 = \frac{k \times (i \times sin\theta - j \times cos\theta)}{i^2 + j^2 + k^2}. \end{cases}$$

The polarization loss factor  $PLF \uparrow$  of the uplink is the squared dot product of the tag's direction t and the polarization vector u. According to (4) and (7), we have:

$$PLF\uparrow(A_m, T, \theta, \beta) = |\mathbf{t}(\beta) \cdot \mathbf{u}(A_m, T, \theta)|^2.$$
 (8)

For the downlink, since the battery-free tag acts as a passive reflector rather than an active transmitter, it cannot actively emit the polarized wave with the linear polarization parallel to the tag's direction. Instead, it just backscatters the reader's radio and the polarization vector of the returned RF wave at T is  $\boldsymbol{u}$  [30]. By projecting  $\boldsymbol{u}$  on the plane that is perpendicular to  $\overrightarrow{TA_m}$  and goes through  $A_m$ , we get the polarization vector of the returned RF wave at  $A_m$ , which is equal to  $\boldsymbol{u}$ . Hence, we have:

$$PLF\downarrow(A_m, T, \theta) = |\boldsymbol{a}(\theta) \cdot \boldsymbol{u}(A_m, T, \theta)|^2. \tag{9}$$

According to (2), (8), and (9), we obtain the PLF of the round-trip RFID communication:

$$PLF = |\mathbf{t}(\beta) \cdot \mathbf{u}(A_m, T, \theta)|^2 \times |\mathbf{a}(\theta) \cdot \mathbf{u}(A_m, T, \theta)|^2,$$
  
=  $|\mathbf{t}(\beta) \cdot (u_1, u_2, u_3)|^2.$  (10)

With this mathematical description of PLF, we show how to estimate the tag's orientation angle  $\beta$  below.

## C. Estimating $\beta$

For each antenna  $A_m$ , we rotate its polarization direction and measure the RSS of the backscattered wave from the tag for N times, each time with a different polarization angle  $\theta$ . In theory, the measured RSS curve will show a peak and a valley over a 180-degree change of  $\theta$ . By finding the maximum of the measured RSS, we can get the angle  $\theta^*$  that corresponds to the peak. The projection of  $\boldsymbol{u}(A_m,T,\theta^*)$  on the x-y plane is the tag's orientation. In other words, we can directly derive an estimate  $\beta^*$  of  $\beta$  according to  $\theta^*$ , i.e.,

$$\beta^* = \arctan(-\frac{u_1(A_m, T, \theta^*)}{u_2(A_m, T, \theta^*)}),\tag{11}$$

where  $u_1$  and  $u_2$  can be seen in (7). This method can quickly pinpoint the tag direction angle  $\beta$  in theory. However, in practice, it suffers from two potential problems. First, the resolution of the RSS measure by the commercial RFID reader is low (0.5dBm for example). This low resolution is easy to produce a plateau of the RSS curve rather than a peak. In other words, there are many different polarization angles that can attain the maximum. It is very likely to cause the accuracy loss if we randomly choose one of them as  $\theta^*$  to derive  $\beta$ . In addition, the thermal noise or unexpected environmental changes might produce an outlier of RSS measure. If this outlier is exactly the maximum, the method of direct derivation will get a wrong estimate. Second, the sampling rate of RSS values for each tag might be low, especially in the case that the reader needs to simultaneously track multiple tags under its coverage and each tag will get only a few chances to be collected. This sparse sampling makes RSS curve contain only a small number of RSS values; the peak in the curve does not indicate the real one, which lowers the estimate accuracy.

The reason of above drawbacks is that the method of direct derivation uses only a single angle  $\theta^*$  (the peak) to estimate  $\beta$ ; other useful information is abandoned. To address this problem, we propose a search-based solution instead. Given a candidate  $\beta'$  of  $\beta$ , we can compute an RSS value  $r'_{m,n}, \forall m \in [1,M], n \in [1,N],$  from (3) for each polarization angle  $\theta_{m,n}$ . We then search the candidate  $\beta'$  (from  $[0,2\pi)$ ) that minimizes the *deviation* (mean squared error) between the computed RSS values  $r'_{m,n}$  and the measured values  $r_{m,n}$ . This angle value, denoted as  $\hat{\beta}$ , is our estimate for  $\beta$ . Hence, the formula for our estimation can be written as:

$$\hat{\beta} = \underset{\beta' \in [0, 2\pi)}{\operatorname{argmin}} \sum_{m=1}^{M} \sqrt{\sum_{n=1}^{N} (r'_{m,n} - r_{m,n})^2}.$$
 (12)

Next we describe how to compute  $r'_{m,n}$ . From (3), we have

$$r'_{m,n} = 10(\lg P_{TX,reader} + \lg C + \lg PLF).$$
 (13)

The value of PLF can be computed from (10). But the value of C depends on many physical parameters of the antenna and the tag, whose precise values are difficult to determine for the following reasons: The values of some physical parameters such as reflection coefficients and antenna gains are often simply not available. One reason is that hardware characteristics may differ amongst individual tags, and it is impractical to calibrate all tags individually. Moreover, even if such parameters are determined for a tag before shipment, their values are typically measured in the anechoic chamber (equivalent to the free space), which may vary significantly from the actual operating environment.

Instead of dealing with the impact of physical parameters individually, we estimate all of them other than PLF as whole. Let  $k_m = 10(\lg P_{TX,reader} + \lg C)$ . Replacing  $r'_{m,n}$  with the measured value  $r_{m,n}$  in (13), we have

$$k_m = r_{m,n} - 10 \times \lg PLF. \tag{14}$$

Taking the average over  $1 \le n \le N$ , we have the following estimate, denoted as  $\hat{k_m}$ :

$$\hat{k_m} = \frac{\sum_{n=1}^{N} (r_{m,n} - 10 \times \lg PLF)}{N}.$$
 (15)

<sup>&</sup>lt;sup>1</sup>When the polarity is mutually orthogonal, the tag cannot capture enough power to activate itself. In this case, the reader will not get any replies from the tag; the valley of the measured RSS curve is not real one of polarity orthogonality. Hence, we choose the peak rather than the valley as the vehicle to derive the tag's orientation angle  $\beta$ .

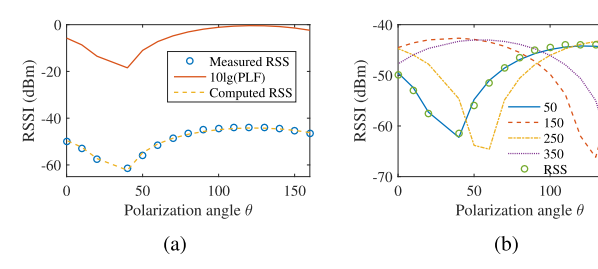


Fig. 4. Theoretical value vs. measured value. (a) Given  $\beta$ , the gap between measured RSS and computed RSS as well as  $10 \lg PLF$ . (b) Computed RSS values under different  $\beta$ s.

Replacing  $k_m$  with  $\hat{k_m}$  in (14), we have

$$r'_{m,n} = \hat{k}_m + 10 \times \lg PLF, \quad 1 \le n \le N.$$
 (16)

We performed extensive experiments with the above formula in the process of determining the tag's orientation angle. We use one example to demonstrate its excellent performance while most experimental results will be presented later. In this experiment, the true value of the tag's orientation angle is  $\beta = 50^{\circ}$ . With 18 RSS values measured from an antenna after every 10° of polarization rotation, we get the real RSS curve under different polarization angles. As shown in Fig. 4(a), the circles are the measured RSS values. According to (10) and (16), we are able to derive  $10 \lg PLF$  and computed RSS for a given  $\beta = 50^{\circ}$ , which are the solid line and the dashed line in Fig. 4(a), respectively. The gap between  $10 \lg PLF$  and the measured RSS is actually a constant caused by the unchanged physical parameters expect PLF during polarization rotation. As we can see, the tightness between the computed RSS and measured RSS well indicates that our proposed model is able to depict the real RSS. In Fig. 4(b), we plot the computed RSS under other tag orientation angles  $(\beta' = 50^{\circ}, 150^{\circ}, 250^{\circ}, 350^{\circ})$  to observe the deviation from measured RSS. The figure shows that as the orientation angle is apart from the ground truth  $(50^{\circ})$ , the deviation gap between the computed value and real value widens, which helps us find the real orientation angle.

To get the estimate of  $\beta$ , we search through the  $\beta'$  values in  $[0,2\pi)$  with a step size of  $0.1^{\circ}$ , and find the optimal estimate  $\hat{\beta}$  based on (12) and (16). Fig. 5 shows the deviation between the computed RSS and the measured RSS with respect to the value of  $\beta'$ . As shown in Fig. 5(a) where one antenna is deployed, the deviation is minimized at  $\beta'=45.8^{\circ}$ . In this case,  $\hat{\beta}=45.8^{\circ}$ , which is very close to the true value of  $50^{\circ}$ . Fig. 5(b) presents the deviations when two reader antennas are deployed. Its estimate is  $\hat{\beta}=46.4^{\circ}$ . As the number of antennas further increases, the estimate will become even closer to the true value. When one (two) antenna is used, the computation time of exhaustive search over the  $\beta'$  values is 4.5 ms (7.6 ms) on a Thinkpad T430s laptop with Intel i5-3210M CPU of 2.50 GHz and 12 GB memory.

# D. Resolving Ambiguity

Tag-Compass however has an *ambiguity* issue, which may sometimes produce an estimate in the opposite direction. Take a closer look at Fig. 5. The deviation of  $\beta'$  actually presents a periodic pattern with period  $\pi$  (180°), i.e., the deviation of  $\beta'$  is about the same as that of  $(\beta' + \pi)$ ,  $0 \le \beta' < \pi$ . Hence, there are two possible estimates with about the same deviation during

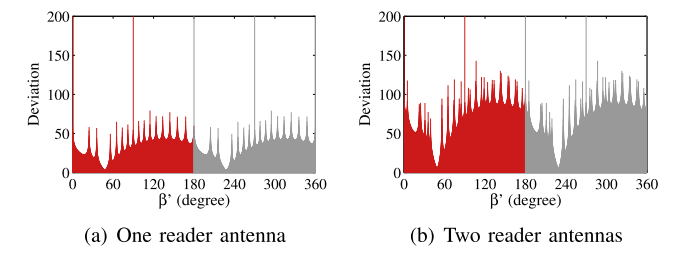


Fig. 5. Deviation between the computed RSS and the measured RSS with respect to the value of  $\beta'$ .

each execution of Tag-Compass, i.e.,  $\hat{\beta}$  and  $\hat{\beta} + \pi$ ,  $0 \le \hat{\beta} < \pi$ . The reason is due to a certain symmetry in placement: The tag is in a plane that is parallel to the plane of each antenna. In this case, if the tag is turned for  $180^{\circ}$ , the physical parameters in (2) for tag-antenna communication do not change. For some applications where the objects themselves are symmetric (such as a symmetric component on an assembly line), this ambiguity will not cause any problem because the objects can be used in either direction. However, in other applications with asymmetric objects, we need to resolve the ambiguity. Formally, we say an estimate  $\hat{\beta}$  is ambiguous if there is at least one angle  $\hat{\beta}'$  (which is far away from  $\hat{\beta}$ ) that makes the deviation between the computed RSS values and the measured ones close to  $\hat{\beta}$ 's. The details about the definition of ambiguity are given below.

Definition 1 (Ambiguity): For an estimate  $\beta$  of the orientation angle based on (12), if there exists another candidate angle  $\beta'$  that meets (17), we say that the estimation is ambiguous.

$$\begin{cases} |\hat{\beta} - \hat{\beta}'| \ge \Omega\\ |D(\hat{\beta}) - D(\hat{\beta}')| \le M \times \Upsilon, \end{cases}$$
 (17)

where M is the number of antennas,  $\Omega$  and  $\Upsilon$  are the angle threshold and the deviation threshold respectively, which are commonly set to  $\Omega = \frac{\pi}{2}$  and  $\Upsilon = 0.5$  in our system.  $D(\beta')$  is the deviation between the computed RSS values  $r'_{m,n}$  and the measured values  $r_{m,n}$  assuming the orientation angle  $\beta$  is equal to  $\beta'$ . Formally,

$$D(\beta') = \sum_{m=1}^{M} \sqrt{\sum_{n=1}^{N} (r'_{m,n}(\beta') - r_{m,n})^2},$$

where  $r'_{m,n}(\beta')$  signifies the value of  $r'_{m,n}$  assuming  $\beta=\beta'$ . If (17) is met, it indicates that both  $\hat{\beta}$  and  $\hat{\beta}'$  are likely to be the actual orientation angle, leading to ambiguity of the estimation. This ambiguity is actually caused by the horizontal placement of the tag deployed on the object. When the tag (tagged object) rotates by  $\pi$  radians from  $\beta$ , the tag direction changes only the vector direction but not the numerical value, i.e.,  $t(\beta) = -t(\beta + \pi)$ . Therefore, we have:

$$PLF(A_m, T, \theta, \beta) = PLF(A_m, T, \theta, \beta + \pi).$$
 (18)

The ambiguity cannot be removed from (18) by increasing the number of antennas. As shown in Fig. 5(b), when multiple antennas are deployed, there are still two candidates both achieving the minimal deviation. To resolve this ambiguity, we are supposed to break the symmetrical relation between  $t(\beta)$  and  $t(\beta + \pi)$ , such that the periodic pattern of  $\pi$  radians is removed. To achieve this goal, we make the plane of the tag

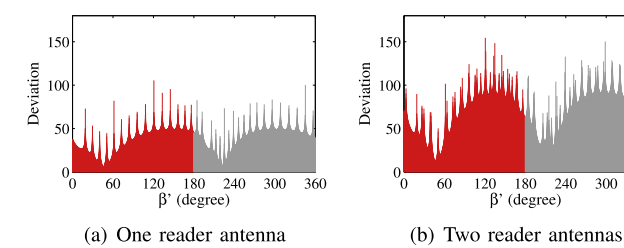


Fig. 6. Deviation between the computed RSS and the real RSS over the value of  $\beta'$  when the tag is inclined.

not parallel to the plane of the antenna. Let  $\alpha$  be the incline angle between the tag direction and the x-y plane, which is preset during the tag deployment, without changing with  $\beta$ . Note that the tag's orientation angle  $\beta$  is now from y-axis to  $\overrightarrow{A'B'}$ , where the points A' and B' are the projection of A and B on the x-y plane, respectively. When the tag rotates by  $\pi$  radians, the vector of the tag direction (including the direction and the numerical value) differs from the case of  $\beta$ . Formally, we have the vector of the tag direction:

$$t(\beta, \alpha) = (-\sin\beta\cos\alpha, \cos\beta\cos\alpha, \sin\alpha). \tag{19}$$

Similar to (10), the round-trip PLF in this case is:

$$PLF = |\boldsymbol{u}(A_m, T, \theta) \cdot \boldsymbol{t}(\beta, \alpha)|^2 \times |\boldsymbol{a}(\theta) \cdot \boldsymbol{u}(A_m, T, \theta)|^2. \quad (20)$$

The rest of the computation is the same as described previously. We repeat the experiment in Fig. 5 with the tag inclined by  $30^{\circ}$ , i.e.,  $\alpha = 30^{\circ}$ . The results are shown in Fig. 6. With a single antenna, the ambiguity is not satisfactorily resolved in Fig. 6(a). Even so, the angular difference between two ambiguous angle estimates is 174.6° rather than 180° ( $\pi$  radians). This angle difference relies on the antenna position. When multiple antennas are deployed, it is hard for each antenna to hold an identical angle difference, which makes the deviation of  $\beta$  much smaller than other angles, effectively resolving the ambiguity (the ambiguity ratio is studied in Section VI-A1). As shown in Fig. 6(b), when two antennas are deployed, only one optimal candidate is left. With the increase of reader antennas, the deviation gap between  $\hat{\beta}$  and the potential ambiguous angle increasingly widens, ensuring unambiguous angle estimation.

# V. DIRECTION FINDING WITH UNKNOWN TAG POSITION

So far, we have discussed the system design of Tag-Compass under the case of knowing the tag's position (in the aforementioned assembly line application, for example). In other applications, such as indoor navigation, the tag's position may not be available at the time of direction finding. In this case, we may locate the tag first by using an existing RFID localization method [2]–[4], and then estimate the tag's orientation angle. This design works but requires extra deployment for localization, which complicates our system. In this section, we perform localization and direction finding together based on the same measurement described in Section III-A, without introducing any extra deployment cost.

For ease of presentation, we present our approach in the 2D plane where the tag resides. The extension to the 3D space (in case that the tag may move vertically) is straightforward by adding one more dimension in searching for an estimated

location of the tag that fits best with the observed data. We partition the surveillance area of interest into a grid of  $L\times W$  squares at cm resolution. The centroid of each square is treated as a candidate position of the tag. The squares are denoted as  $S_{l,w}$ . We build three types of holograms: 1) RSS hologram, 2) Angle hologram, and 3) RSS-Angle hologram, in order to find the square at which the tag is located and then determine the tag's orientation angle meanwhile.

## A. RSS Hologram

The rationale of RSS Hologram (RH) is explained as follows: For each square  $S_{l,w}$ ,  $1 \leq l \leq L$ ,  $1 \leq w \leq W$ , we use its centroid as the tag position and obtain an estimate  $\hat{\beta}_{l,w}$  value for the tag's orientation angle from (12). Among these estimate values, we find the one with the smallest deviation between the computed RSS values and the measured RSS ones and use that value as the final estimated orientation angle  $\hat{\beta}$ . And we use the centroid of the corresponding square as the estimated tag position. Based on the above idea, we build an RSS deviation-based image exhibition as follows.

$$RH = \begin{pmatrix} h_{1,1}^r & . & h_{1,W}^r \\ . & . & . \\ h_{L,1}^r & . & h_{L,W}^r \end{pmatrix}.$$
 (21)

RH consists of  $L \times W$  pixels. Each pixel  $h_{l,w}^r$  is the minimal deviation between the measured RSS values and the computed RSS values, assuming the tag is located in the square  $S_{l,w}$ . It is called RSS deviation:

$$h_{l,w}^r = \min \sum_{m=1}^M \sqrt{\sum_{n=1}^N (r'_{m,n} - r_{m,n})^2},$$
 (22)

where  $r_{m,n}$  is the *n*th measured RSS value by the *m*th antenna and  $r'_{m,n}$  is the corresponding computed value from (16). According to (12), the estimate angle  $\hat{\beta}_{l,w}$  at square  $S_{l,w}$  is:

$$\hat{\beta}_{l,w} = \underset{\beta' \in [0,2\pi)}{\operatorname{argmin}} \sum_{m=1}^{M} \sqrt{\sum_{n=1}^{N} (r'_{m,n} - r_{m,n})^2}.$$
 (23)

Among the  $L \times W$  squares, the one  $S_{l,w}$  with the minimal pixel value  $h_{l,w}^r$  is considered to contain the tag, and the corresponding  $\hat{\beta}_{l,w}$  is used as the final estimate for the tag's orientation angle. Formally, we have the estimate  $\hat{\beta}$  as follows:

$$\hat{\beta} = \hat{\beta}_{l,w}, \text{ where } [l, w] = \underset{1 < l < L; 1 < w < W}{\operatorname{argmin}} (h_{l,w}^r).$$
 (24)

We show the results of an experimental study with three linearly polarized antennas in Fig. 7, where the antennas cover a 2D plane of  $200cm \times 200cm$ . The tag is located at the origin (0,0) with an incline angle of  $30^{\circ}$ . The distance between the tag and the antenna plane is 1.5m and the true orientation angle of the tag is  $50^{\circ}$ . The step size of the orientation angles and the edge length of each square are set to  $0.5^{\circ}$  and 2cm, respectively. The RH is built according to (21), as shown in Fig. 7(a). Each pixel in this image is the normalized result and the blue colors denote small deviation values. The estimated tag position is (-14, -18)cm and the corresponding orientation angle is  $56.8^{\circ}$ , which are close to the real values. Although RH achieves good localization and angle

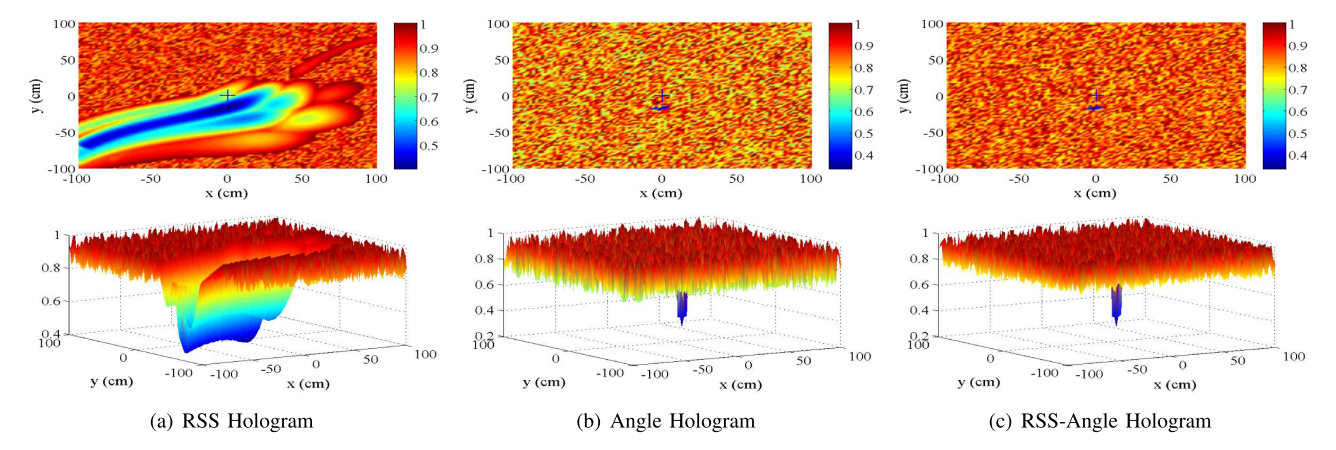


Fig. 7. **Tag-Compass Holograms**. An image exhibition that depicts the likelihood of a square to be the tag position. The smaller the pixel value is, the more likely the square contains the tag. Three columns show RH/AH/RAH in 2D/3D images.

estimate, there is a large stretch of the blue area with small deviation values, which may sometimes degrade the accuracy in localization and angle estimate. Below we propose a more reliable method.

# B. Angle Hologram

For each square  $S_{l,w}$ ,  $1 \le l \le L$ ,  $1 \le w \le W$ , we use its centroid as the tag position and then use the measured RSS values from each antenna to make a separate estimate for the tag's orientation angle — there will be M estimates for M antennas. If  $S_{l,w}$  contains the tag, all M estimates will be close to each other. Otherwise, the estimates will be different. This difference, captured by *angle variance* below, is dependent on how far the square is away from the true position of the tag. We build Angle Hologram (AH) below:

$$AH = \begin{pmatrix} h_{1,1}^{a} & . & h_{1,W}^{a} \\ . & . & . \\ h_{L,1}^{a} & . & h_{L,W}^{a} \end{pmatrix}.$$
 (25)

where each pixel  $h_{l,w}^a$  records the variance of the M estimates of the tag's orientation angle computed based on the measurements from the M antennas, assuming the tag is located at the square  $S_{l,w}$ . This variance is called *angle variance*:

$$h_{l,w}^{a} = \frac{1}{M} \sum_{m=1}^{M} (\hat{\beta}_{l,w}(A_m) - \mu_{l,w})^2,$$
 (26)

where

$$\begin{cases} \mu_{l,w} = d \frac{1}{M} \sum_{m=1}^{M} \hat{\beta}_{l,w}(A_m) \\ \hat{\beta}_{l,w}(A_m) = \underset{\beta \in [0,2\pi)}{\operatorname{argmin}} \sum_{n=1}^{N} (r'_{m,n} - r_{m,n})^2. \end{cases}$$
(27)

The term  $\hat{\beta}_{l,w}(A_m)$  is the estimate of the orientation angle based on the RSS measurements from the antenna  $A_m$ , and  $\mu_{l,w}$  is the mean of the M estimates by the M antennas. If the square  $S_{l,w}$  contains the tag position, the variance  $h^a_{l,w}$  will be smaller than those of other squares. Hence, we use the square  $S_{l,w}$  with the minimal  $h^a_{l,w}$  value to estimate the tag's location. The final estimate  $\hat{\beta}$  of the tag's orientation angle is as follows.

$$\hat{\beta} = \mu_{l,w}, \text{ where } [l,w] = \underset{1 \le l \le L; 1 \le w \le W}{\operatorname{argmin}} (h_{l,w}^a).$$
 (28)

However, there is the ambiguity issue when we use one antenna  $A_m$  to find the orientation angle  $\hat{\beta}_{l,w}(A_m)$ ; see Section IV-D. To solve this problem, we compute  $\hat{\beta}_{l,w}$  via (23) first for each square  $S_{l,w}$ , which does not have the ambiguity issue because all M antennas are used. We then compute  $\hat{\beta}_{l,w}(A_m)$ ; if ambiguity arises, we choose the value that is closer to  $\hat{\beta}_{l,w}$ . It may appear that AH will take much longer time than RH to compute, but in reality that is not the case. Most of the computation for  $\hat{\beta}_{l,w}(A_m)$ ,  $1 \leq m \leq M$ , can benefit from the intermediate results in computing  $\hat{\beta}_{l,w}$ . Hence, we find in our implementation that AH takes almost the same time as RH, with negligible difference.

Fig. 7(b) shows the AH under the same experimental setting as in Fig. 7(a). Clearly, only a small patch of blue zone is left with small deviation values, effectively excluding all squares that are not close to the tag at (0,0). With AH, the estimated tag position is (-8,-18)cm and the orientation angle is  $56.2^{\circ}$ .

# C. RSS-Angle Hologram

RH and AH provide two metrics, RSS deviation and angle variance, for estimating the tag's position and orientation angle. We take a further step to combine them for an RSS-Angle Hologram (RAH), as defined below.

$$RAH = \begin{pmatrix} h_{1,1} & . & h_{1,W} \\ . & . & . \\ h_{L,1} & . & h_{L,W} \end{pmatrix}.$$
 (29)

Each pixel  $h_{l,w}$  is calculated as follows:

$$h_{l,w} = h_{l,w}^r \times h_{l,w}^a, \tag{30}$$

where  $h_{l,w}^r$  and  $h_{l,w}^a$  are calculated by (22) and (26), respectively. As previously mentioned, smaller  $h_{l,w}^r$  and  $h_{l,w}^a$  values indicate higher likelihood to contain the tag position. Hence, we use the square  $S_{l,w}$  with the minimal  $h_{l,w}$  value as an estimate for the tag's location:

$$[l, w] = \underset{1 < l < L: 1 < w < W}{\operatorname{argmin}} (h_{l, w}). \tag{31}$$

After this square is determined, we estimate the orientation angle in the following.

$$\hat{\beta} = \frac{1}{2}(\hat{\beta}_{l,w} + \mu_{l,w}),\tag{32}$$

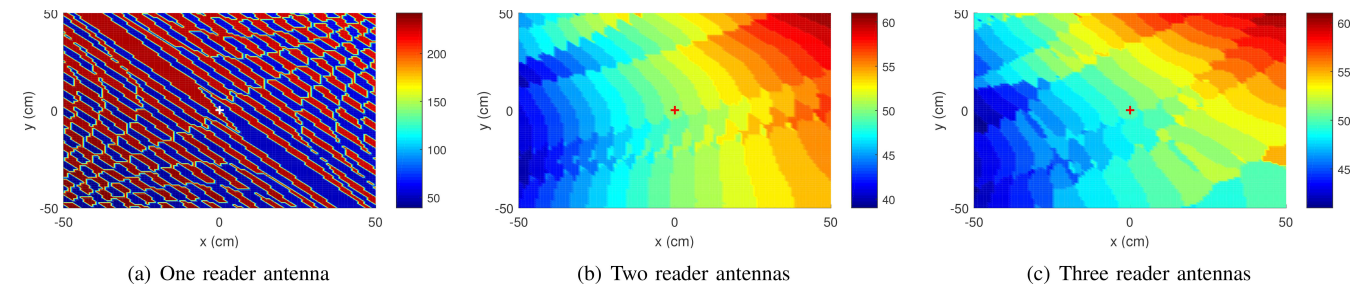


Fig. 8. Relationship between the localization accuracy and the angle estimate of  $\beta$ .

where  $\hat{\beta}_{l,w}$  and  $\mu_{l,w}$  can be calculated by (23) and (27), respectively. Fig. 7(c) presents the RAH under the same experimental deployment as in Fig. 7(a) and Fig. 7(b). RAH not only keeps a small blue area as AH, but also widens the likelihood gap between blue area and other area. With RAH, the estimated tag position is (-6, -16)cm and the estimated orientation angle is  $55.4^{\circ}$ , very close to the true values.

# D. Localization vs. Angle Estimate

An interesting fact from above experiment results is that the accurate angle estimation is achieved on the top of localization results with deviations. This may indicate that the angle estimate by Tag-Compass is insensitive to the tag localization. To verify this conclusion, we next study the relationship between angle estimate and tag localization. Suppose the tag is located at the origin (0,0) with an incline angle of  $30^{\circ}$ . The height difference between the tag and the reader antenna is 2.0m and the true orientation angle of the tag is  $50^{\circ}$ . In theory, the measured RSS can be computed by adding a constant and  $10 \lg PLF$ . Now, we observe a  $100cm \times 100cm$ neighbor area of the origin (0,0). For each position, we assume some deviations of the tag localization happen and the tag is exactly located at that point (although the ground truth is the origin), we can obtain the theoretical RSS values under different polarization angles according to (20).

As shown in Fig. 8(a), each plot is the angle estimate of  $\beta$  under the assumption that the tag is located at that point. As we can see, even the position, e.g., (50, 0)cm, is far away from the real tag position (0,0), the angle estimate is still close to the truth (blue area). The red zone that is far away from the real angle is due to the angle ambiguity discussed in Section IV-D. When multiple reader antennas are deployed, this issue can be well addressed. As shown in Fig. 8(b) and Fig. 8(c), when two and three antennas are deployed respectively, the errors of the estimated angles at different positions are bounded in the range of  $[-10^{\circ}, 12^{\circ}]$ , even the position is far away from the origin, e.g., (50, 50)cm. In other words, some localization deviations will not have a great impact on the angle estimate, which ensures the accurate angle estimation even with some localization deviations.

## E. Reducing Computation Overhead

The computations involved in building RH/AH/RAH may introduce much overhead, which thereby affects the real-time capability of pose sensing. This might be more severe when the surveillance area is larger or the tag moves in the 3D space. Hence, we in this subsection improve the time efficiency of

Tag-Compass by using the schemes of hashtable, hierarchical search, and search space reduction.

- 1) Hashtable: Considering the building of RH/AH/RAH, we find that much computation overhead is consumed to derive the theoretical polarization loss factor  $10 \lg PLF$ . To avoid most of this overhead, for each square, we can pre-compute the PLFs under each tag rotation angle and each reader antenna's polarization angle. Although this may take dozens of seconds, it executes only once in an off-line way and the PLF results are stored in a hashtable. When starting to on-line sense the object's pose, we can search the corresponding items in the hashtable to obtain the PLFs for each square; no PLF computation is needed. This approach will greatly reduce the global computation overhead.
- 2) Hierarchical Search: Fine-grained partition of the surveillance area produces accurate estimate results, but suffers from high computation overhead. To reduce the overhead, we adopt two-level hierarchical search that begins with a coarse-grained area partition in order to quickly locate a large square where the tag resides, and then partitions the large square into small squares and performs the search a second time for accurate estimation of tag location and orientation angle. This search strategy can be generalized to more than two levels. Our experiment results show that the hierarchical search can dramatically speed up hologram building to less than half a second, at a small expense of accuracy loss.
- 3) Search Space Reduction: For estimating  $\beta$ , we need to do the brute-force search over a full 360-degree angle space, which is time consuming. To reduce this overhead, we can resort to the method of direct derivation. More specifically, by running (11) first, we can quickly find a potential candidate  $\beta^*$  of the tag's orientation angle. After that, we do the brute-force search over a small interval around  $\beta^*$ , instead of  $[0,2\pi)$ . In other words, the full search space of  $[0,2\pi)$  can be reduced to the interval  $[\beta^* \xi, \beta^* + \xi]$ , where  $\xi$  is a threshold that is set to 30 degrees in this paper. This will simplify our algorithm and accelerate the computation.

## VI. IMPLEMENTATION & EVALUATION

We develop a prototype of Tag-Compass to evaluate the system performance, as shown in Fig. 9.

Reader: The reader that we use is an Impinj Speedway R420 [27], which provides four RP-TNC ports to support four antenna connections at most. If more than four antennas are required, we can resort to an Antenna Hub [27] that allows a single reader to connect up to 32 antennas. In our experiments, we deploy five antennas at most to evaluate our system. We stress that although the maximum number of antennas goes



Fig. 9. Experiment setups.

beyond four, we believe in practice one through four antennas will be sufficient, depending on the application requirements on ambiguity resolution and direction-estimation accuracy.

Antennas: We choose Larid PA9-12 and PAV90209H-FNF antennas [28] as our linearly polarized antennas. These antennas are hung from the holders on a gantry and uniformly scheduled by the reader in round robin [4]. Each holder is equipped with a servo motor that can rotate the antenna continuously. Each antenna is parallel to the x-y plane and faces to -z-axis. The positions of the five antennas are (0, 0, 150)cm, (-50, 0, 150)cm, (50, 0, 150)cm, (0, -50, 150)cm, and (0, 50, 150)cm, respectively. In practice, one may want to use the technique of dynamic polarization control (DPC) [31] to set the polarization of the far-field electric field generated by a radiating antenna in an electronically controlled manner, without any mechanical configuration. For example, by controlling the amplitude and the phase, Bowers et al. [31] designed a DPC-enabled antenna that is able to electronically change the polarization angle across the entire tuning range of  $0^{\circ}$  to  $180^{\circ}$ .

Tags: On the top of an object, we attach a dipole ALN 9640 tag [24], which is sensitive to the polarization of the incoming waves. The tag's position distributes randomly in the x-y plane with the coordinate  $(x_t, y_t, 0)$ cm, where  $x_t \in [-100, 100]$  and  $y_t \in [-100, 100]$ .

Based on the above deployment, we evaluate the performance of our system in two cases: 1) known tag position and 2) unknown tag position.

# A. Evaluation With Tag Position

1) Ambiguity: In Fig. 10, we show the ambiguity ratio of Tag-Compass with respect to the number of antennas. The ambiguity ratio is defined as the proportion of the number of ambiguous estimates (there exist two angles  $\beta$  and another angle around  $(\beta + \pi)$  both minimize the deviation) and that of all estimates. As shown in this figure, when a single antenna is deployed, ambiguity happens in most cases. However, as the number of antennas increases, the ambiguity ratio is quickly reduced. For example, with two antennas, the ambiguity ratio drops to 6.7%. When three or more antennas are deployed, the ambiguity disappears completely. The reason is that, for two angles that happen to both minimize the deviation between computed RSS and measured RSS for one antenna, the chance for them to also both minimize the deviation for any other antenna is very small, because the polarization properties associated with these antennas are all different due to their different placement. We stress that this ambiguity will not

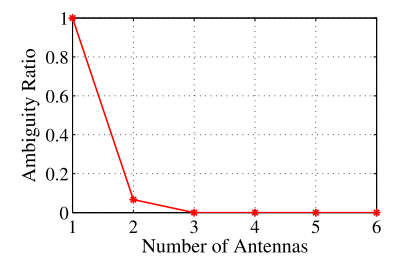


Fig. 10. Ambiguity.

cause any problem in the applications that the objects can be used in either direction (such as a symmetric component on an assembly line). However, in other applications with asymmetric objects, we need to resolve the ambiguity. Hence, to be applicable to all cases, the number of reader antennas used below is no less than three, completely avoiding ambiguity.

2) Accuracy: The most related work is RF-Compass [22] that uses iterative space partition to identify an object's orientation. As is explained in the introduction, RF-Compass involves two tags on the object and several tags on a robot that approaches towards the object. Essentially, it uses the tags on the robot to help locate the two tags on the object through the space-partitioning technique. Once the approximate locations of two tags on the object are known, the line segment between these locations provides a reference for the object's orientation. This will not work well if the objection's dimensions are small so that the tags are close to each other. RF-Compass is designed for a specific robotic setting, whereas this paper studies the general problem of direction finding. Therefore, in order to make comparison in the context of this paper, we simplify and improve the performance of RF-Compass by removing the robot of several tags and instead using the more advanced tag-localization algorithms, PinIt [3] and DAH [4], which will give more accurate tag coordinates and thus give better estimate of the tag's direction. As we demonstrate below, except for large objects of sizes in meters, the start-of-the-art algorithms do not provide sufficient localization precision for direction finding.

Modified RF-compass with PinIt: In the experiment, we let the two tags on the object be 20cm apart. PinIt [3] exploits a tag's multipath profile to locate it. The underlying rationale behind PinIt is that nearby tags experience a similar multipath environment and thus exhibit similar multipath profile. PinIt aims to estimate the tag position in a manner robust to multipath and non-line-of-sight, but it needs an antenna array (or a mobile antenna) and many references tags to cover the surveillance area. According to [3], PinIt achieves a median error of 11.2cm in localization, with a standard deviation of 6.2cm. Applying it on direction finding, our experiment shows that it has a mean error of 30.0° with a standard deviation of 23.2°, as shown in Fig. 11. We want to stress that this result does not at all mean that RF-Compass has a questionable design. On the contrary, it is a great design in its context where iterative adjustment of robot movement is used to compensate the inaccuracy in direction finding. However, in a more general non-robotic context with smaller objects, we need better tools for direction finding.

Modified RF-compass with DAH: DAH [4] builds a differential augmented hologram using the phase values for localizing a tag. Compared with PinIt, DAH is more scalable in

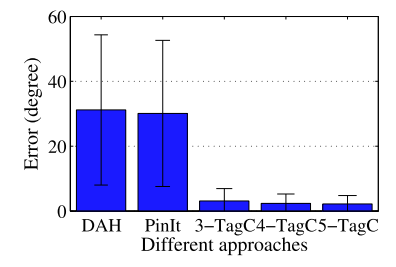


Fig. 11. Accuracy comparison.

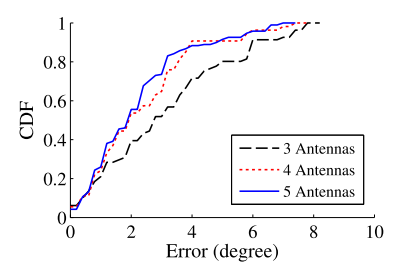


Fig. 12. CDF of accuracy.

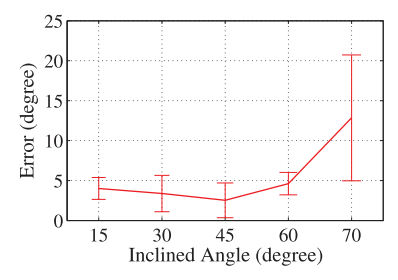


Fig. 13. Impact of  $\alpha$ .

RFID applications as it does not need to pre-deploy reference tags for accurate calibration. It needs multiple antennas and requires the object (or the antennas) to be moving in order to locate the tag. In the case where the tag's trajectory is unknown, DAH has a median error of 12.3cm in localization, with a standard deviation of 5cm. Applying it on direction finding, our experiment shows that DAH has a mean error of  $31.6^{\circ}$  with a standard deviation of  $21.5^{\circ}$ , as shown in Fig. 11.

Tag-compass: In Fig. 11, when three antennas are deployed, Tag-Compass has a median error of 3.1° in direction finding, with a standard deviation of 3.8°; when four antennas are deployed, Tag-Compass has a median error of 2.5° in direction finding, with a standard deviation of 1.7°, outperforming DAH and PinIt by 12.6 times and 12.0 times, respectively. Taking a closer look at the accuracy comparison, Fig. 12 plots the CDFs of the estimate error by Tag-Compass. With four antennas, Tag-Compass's 90th percentile is 4.3°, and 99th percentile is 7.0°, achieving high precision within a few degrees. The estimation accuracy will be further improved as the number of antennas increases. This performance benefits from high sensitivity of dipole tags to polarization orientation.

3) Impact of Incline Angle: The inclined tag helps to resolve the ambiguity issue as aforementioned. We check whether the incline angle  $\alpha$  has impacts on the accuracy of Tag-Compass. Fig. 13 depicts the accuracy with respect to the incline angles ranging from  $15^{\circ}$  to  $75^{\circ}$ . In the figure, the angle error almost remains stable first as the incline angle increases. This indicates that the accuracy is irrelevant to the incline angle when the incline angle is within a threshold ( $60^{\circ}$  in our experiment). When the incline angle exceeds the threshold,

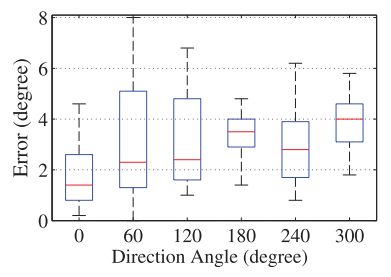


Fig. 14. Impact of  $\beta$ .

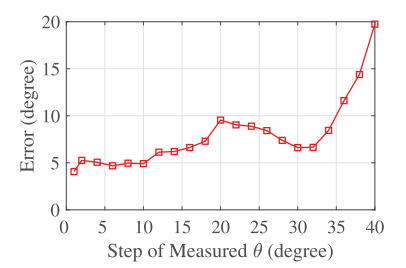


Fig. 15. Impact of  $\theta$ 's step.

the angle error increases sharply. That is because the big incline angle weakens the changes of RSS caused by antenna rotation, thereby degrading the estimate accuracy. Consider an extreme case where the incline angle is  $90^{\circ}$  and the reader antenna is right above the tag. The included angle between the tag direction and the antenna polarization always keeps unchanged ( $90^{\circ}$ ) as the antenna rotates, disabling the ability of direction finding. Besides, the received power decreases as the incline angle increases. To trade off the accuracy, ambiguity issue, and the received power, we empirically set the incline angle to  $30^{\circ}$  in our system.

4) Impact of Orientation Angle: In Fig. 14, we study the estimate accuracy of Tag-Compass with respect to the orientation angles. The tag inclines 30° and rotates from 0° to 360°, with a step of 60°. In each orientation angle, we deploy four antennas to identify this tag's orientation angle. As shown in this figure, the tightness (small errors) between the estimated value and the real value well indicates that Tag-Compass can achieve a high resolution of estimation under different orientation angles.

5) Impact of  $\theta$ 's Rotation Step: In Fig. 15, we study how the rotation step of the measured  $\theta$  affects the estimate accuracy. We fix the rotation interval of  $\theta$  to  $[0,180^\circ]$  and vary the rotation step of  $\theta$  from 2 degrees to 40 degrees. In each experiment, we deploy four antennas to identify this tag's orientation angle  $\beta$ . As shown in this figure, the estimate error almost remains stable as the step increases (when the step is small). After that, the error experiences a rise trend over the steps in general. The reason is that small steps will get more RSS samples which benefit the estimation of  $\beta$ . Note that, although the small step attains higher accuracy, it suffers from higher computation overhead. This is a tradeoff between time efficiency and estimate accuracy, depending on the application requirements.

6) Impact of  $\theta$ 's Rotation Range: In Fig. 16, we study the impact of the  $\theta$ 's rotation range on the estimate accuracy. We fix the rotation step of  $\theta$  to 2 degrees and vary the ranges of  $\theta$  from  $[0,10^\circ]$  to  $[0,180^\circ]$ . It clearly shows that the error decreases as the range increases. That is because large interval benefits in widening the gap between different RSS

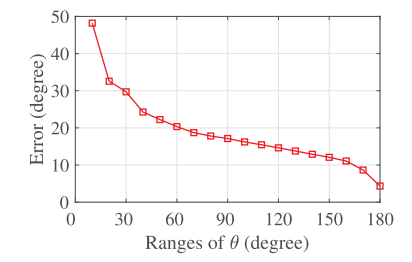


Fig. 16. Impact of  $\theta$ 's range.

measurements, which helps screen out the wrong candidates and get the real estimate more easily.

## B. Evaluation Without Tag Position

In the following experiments, we study the performance of Tag-Compass to sense the tag's pose without the assumption of knowing the tag position in advance.

1) Localization Accuracy: Fig. 17 depicts the localization accuracy of RAH under different scenarios, where three, four, and five antennas are respectively deployed to cover a surveillance region with the size of  $200cm \times 200cm$ . The tag is located at the origin (0,0). For a given number of antennas, we conduct 50 groups of experiments to evaluate the localization accuracy in x-axis, y-axis, and the 2D plane (under the label "combined" in the figure). As shown in this figure, when three antennas (3-RAH) are used, our method RAH achieves a mean error of 21.2cm, 23.4cm, and 35.3cm in above dimensions, outperforming most RSS-based localization algorithms. With the increase of antennas, the localization accuracy of RAH increasingly improves in all three dimensions. For example, with five antennas (5-RAH), our approach achieves the localization with mean error of 15.4cm, 8.5cm, and 18.7cm in x-axis, y-axis, and 2D plane. This is a great improvement on the localization accuracy compared with 3-RAH, much close to the state-of-the-art PinIT [3] and DAH [4]. We assert that Tag-Compass provides a novel and accurate RSS-based localization technique, with no need of any reference tag deployment.

2) Accuracy of Estimating  $\beta$ : In Fig. 18, we study the accuracy of RH, AH, and RAH in estimating the orientation angle  $\beta$  of the tag. When three antennas are deployed in Fig. 18(a), RAH performs best, RH and AH follow and perform equally well. With the increase of antennas, the estimation accuracy of RH, AH, and RAH improves significantly. For example, RAH with four antennas achieves a median error of 3.8°, with the standard variance 3.6°, as shown in Fig. 18(b). Note that RH is much worse than others as the number of antennas increases. That is because the holograms provide different localization results under different antenna deployment. These results are close to, but not exactly the same as, the real tag position. It is hard for RH's angle estimate in a position to closely resemble that in another different position. By contrast, each antenna in AH individually searches the optimal angle which is randomly distributed around the ground truth. The mean of all estimated angles enables AH to decrease the variance, thereby performing better than RH. In conclusion, our proposed three holograms can achieve accurate direction finding with no priori knowledge of the tag position. This high performance also demonstrates that our estimate approach is able to tolerate the localization deviation to some degree.

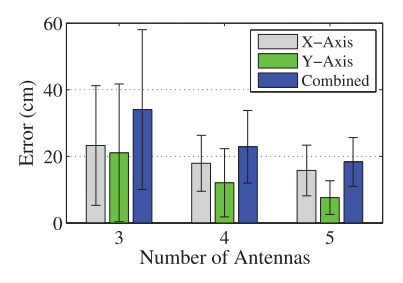


Fig. 17. RAH-based localization.

3) Hierarchical Search: In this experiment, we investigate the performance gain as well as the accuracy loss of the hierarchical search, compared with that of the fine-grained one-level search. In the fine-grained search, the edge length of the squares is set to 2cm and the step size of the angle search is set to 0.5°. In the two-level hierarchical search, we set the parameters as follows: At the first level, we set the edge length to 20cm, and the step size of the angle to 1°. After finding the square with minimum deviation, at the second level, we zoom in to this square and search the  $20cm \times 20cm$  area using the same granularity as the finegrained search. Under this setting, we compare the execution time of the both search methods: When four antennas are deployed, the hierarchical search takes only 0.34s to build RAH for localization and angle estimation, which obtains about 70× performance gain compared with 23.2s of the finegrained search. Besides, we check the accuracy loss of the hierarchical search. Fig. 19(a) depicts the localization accuracy of RAH under different number of antennas. As we can see, the fine-grained search only slightly outperforms the hierarchical search. The similar conclusion can also be drawn on the angle estimation, as shown in Fig. 19(b). To sum up, we say that the hierarchical search can greatly speed up the execution of Tag-Compass, at a very small expense of accuracy loss.

## VII. RELATED WORK

The problem of identifying an object's spatial pose with RFID has not received adequate attention. In traditional RFID localization, the RFID tag is viewed as a particle; orientation information is not taken into account. SpotON [32] is one of the earliest localization systems using RFID. By designing and customizing tags, it can utilize radio signal attenuation to estimate the inter-tag distance and locate tag's position more accurate than the triangulate method. LANDMARC [2] dynamically adjusts the reader's transmit power and weights the knearest reference tags' locations to estimate the target tag's position. Lee and Lee [33] consider a case of mobile robot and use RFID tag array to reduce the accumulated errors caused by robot movement. Maneesilp et al. [34] propose a passive scheme and an active scheme to pinpoint an object in 3D space. PinIt [3] exploits a tag's multipath profile to locate it. The underlying rationale behind PinIt is that nearby tags experience a similar multipath environment and thus exhibit similar multipath profile. DAH [4] builds a differential augmented hologram using the phase values for localizing a tag. Compared with PinIt, DAH is more scalable in RFID applications as it does not need to pre-deploy reference tags for accurate calibration. Although above algorithms greatly improve the indoor localization accuracies, they cannot identify the tag's orientation. The scheme of deploying multiple tags to estimate

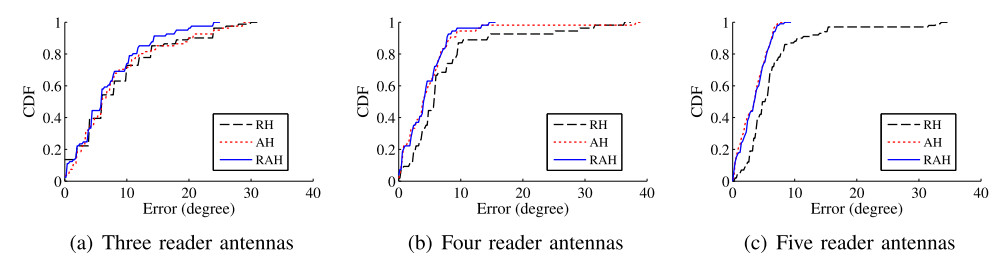


Fig. 18. Accuracy of angle estimation without tag position.

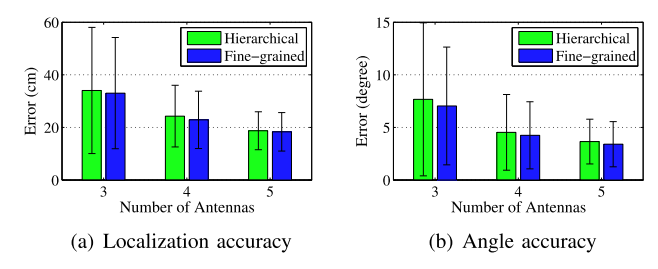


Fig. 19. Hierarchical search vs. fine-grained search.

the object's orientation is also inadequate, especially for small size objects where the tags must be placed close.

In recent years, some research starts to focus on the other half of pose sensing: identifying the object's orientation. RF-Compass [22] is tailored to the specific application of robotic assembly. Although RF-Compass achieves high accuracy through a space partitioning technique, it is designed for the specific robotic setting and needs a robot to continuously move towards the target, which is not a general solution to direction finding. Tagyro [35] tracks the 3D orientation of passive objects using RFID tags. The basic idea is to attach multiple tags to different spots on the object, which constitute a tag array. When the tag array rotates together with the object, the tag-to-reader distance among different tags varies, which in turn affects the relative phase offset between tags (referred to as PDoA). Tagyro builds a closed-form model that transforms PDoA into an orientation spectrum, which characterizes the likelihood of each orientation angle. However, the tag array needs to be carefully deployed and also the object movement is not allowed, which limits the applications.

PolarDraw [36] improves the tracking accuracy of a pen's movement trajectory by combining the phase value and the polarization. The phase trends to estimate the moving distance of the pen and the polarization is used to estimate pen direction. However, it just gives a rough estimation of the tag's orientation rather than a fine-grained angle in our work. Krigslund et al. [37] design a Bayesian estimator to identify the tag inclination based on the polarization attributes. By decomposing the received signal into two orthogonal signal components, they can determine the polarization of received signal, so does the tag's orientation. This design, however, suffers from three main problems. First, the system deployment is unscalable. It requires the tag to be placed at the center of a circle and all antennas to be evenly spaced in the circle, which makes the system unable to track multiple tags concurrently. Second, this study cannot work properly without the tag's position. Third, the assumption that the received signals experience approximately the same multi-path fading amongst all antennas is unreasonable. That is because, the antennas are far apart from each other. It is hard for

them to get the similar multi-path fading, especially in the indoor environment. As a follow-up work, Krigslund *et al.* [38] use the polarization for the first time to capture the human movement. However, this work does not figure out the relationship between the polarization properties of the RF waves and the tag's orientation in the 3D space. Besides, it cannot pinpoint the tag's position with the polarization.

# VIII. CONCLUSION

In this paper, we propose Tag-Compass, a fine-grained pose sensing system. The key innovation of Tag-Compass is to determine an object's orientation by estimating the direction of a single RFID tag based on the polarization properties of electromagnetic waves. We develop an insight into the relationship between the RSS values and the tag direction and apply this insight to estimate the latter through a series of transformations and deviation minimization. Extensive experiments demonstrate that Tag-Compass can estimate a tagged object's orientation with an error of only a few degrees and pinpoint the object's position accurately.

## REFERENCES

- [1] J. Liu, M. Chen, S. Chen, Q. Pan, and L. Chen, "Tag-compass: Determining the spatial direction of an object with small dimensions," in *Proc. IEEE INFOCOM-IEEE Conf. Comput. Commun.*, May 2017, pp. 1–9.
- [2] L. M. Ni, Y. Liu, Y. C. Lau, and A. P. Patil, "LANDMARC: Indoor location sensing using active RFID," in *Proc. 1st IEEE Int. Conf. Pervasive Comput. Commun. (PerCom)*, Mar. 2003, pp. 407–415.
- [3] J. Wang and D. Katabi, "Dude, where's my card?: RFID positioning that works with multipath and non-line of sight," in *Proc. ACM SIGCOMM Conf. SIGCOMM (SIGCOMM)*, 2013, pp. 51–62.
- [4] L. Yang, Y. Chen, X.-Y. Li, C. Xiao, M. Li, and Y. Liu, "Tagoram: Real-time tracking of mobile RFID tags to high precision using COTS devices," in *Proc. 20th Annu. Int. Conf. Mobile Comput. Netw. (Mobi-Com)*, 2014, pp. 237–248.
- [5] L. Shangguan, Z. Yang, A. X. Liu, Z. Zhou, and Y. Liu, "Relative localization of RFID tags using spatial-temporal phase profiling," in *Proc. USENIX NSDI*, 2015, pp. 251–263.
- [6] J. Han et al., "Twins: Device-free object tracking using passive tags," IEEE/ACM Trans. Netw., vol. 24, no. 3, pp. 1605–1617, Jun. 2016.
- [7] G. Wang et al., "HMRL: Relative localization of RFID tags with static devices," in Proc. 14th Annu. IEEE Int. Conf. Sens., Commun., Netw. (SECON), Jun. 2017, pp. 1–9.
- [8] C.-H. Lee and C.-W. Chung, "RFID data processing in supply chain management using a path encoding scheme," *IEEE Trans. Knowl. Data Eng.*, vol. 23, no. 5, pp. 742–758, May 2011.
- [9] S. Qi, Y. Zheng, M. Li, Y. Liu, and J. Qiu, "Scalable industry data access control in RFID-enabled supply chain," *IEEE/ACM Trans. Netw.*, vol. 24, no. 6, pp. 3551–3564, Dec. 2016.
- [10] J. Liu, B. Xiao, K. Bu, and L. Chen, "Efficient distributed query processing in large RFID-enabled supply chains," in *Proc. IEEE INFOCOM-IEEE Conf. Comput. Commun.*, Apr. 2014, pp. 163–171.
- [11] C. Qian, H. Ngan, Y. Liu, and L. M. Ni, "Cardinality estimation for large-scale RFID systems," *IEEE Trans. Parallel Distrib. Syst.*, vol. 22, no. 9, pp. 1441–1454, Sep. 2011.

- [12] X. Liu, S. Zhang, B. Xiao, and K. Bu, "Flexible and time-efficient tag scanning with handheld readers," *IEEE Trans. Mobile Comput.*, vol. 15, no. 4, pp. 840–852, Apr. 2016.
- [13] J. Liu, M. Chen, B. Xiao, F. Zhu, S. Chen, and L. Chen, "Efficient RFID grouping protocols," *IEEE/ACM Trans. Netw.*, vol. 24, no. 5, pp. 3177–3190, Oct. 2016.
- [14] X. Liu et al., "Fast RFID sensory data collection: Trade-off between computation and communication costs," IEEE/ACM Trans. Netw., vol. 27, no. 3, pp. 1179–1191, Jun. 2019.
- [15] L. Xie et al., "TaggedAR: An RFID-based approach for recognition of multiple tagged objects in augmented reality systems," *IEEE Trans. Mobile Comput.*, vol. 18, no. 5, pp. 1188–1202, May 2019.
- [16] J. Yu, W. Gong, J. Liu, L. Chen, and K. Wang, "On efficient tree-based tag search in large-scale RFID systems," *IEEE/ACM Trans. Netw.*, vol. 27, no. 1, pp. 42–55, Feb. 2019.
- [17] S. Jorg, J. Langwald, J. Stelter, G. Hirzinger, and C. Natale, "Flexible robot-assembly using a multi-sensory approach," in *Proc. ICRA. Millennium Conf. IEEE Int. Conf. Robot. Automation. Symposia*, vol. 4, Apr. 2000, pp. 3687–3694.
- [18] M. Bonert, L. H. Shu, and B. Benhabib, "Motion planning for multirobot assembly systems," *Int. J. Comput. Integr. Manuf.*, vol. 13, no. 4, pp. 301–310, Jan. 2000.
- [19] M. Kim and N. Y. Chong, "RFID-based mobile robot guidance to a stationary target," *Mechatronics*, vol. 17, nos. 4–5, pp. 217–229, May 2007.
- [20] M. Kim, H. W. Kim, and N. Y. Chong, "Automated robot docking using direction sensing RFID," in *Proc. IEEE Int. Conf. Robot. Autom.*, Apr. 2007, pp. 4588–4593.
- [21] P. Corke, Robotics, Vision and Control: Fundamental Algorithms in MATLAB. New York, NY, USA: Springer, 2011.
- [22] J. Wang, F. Adib, R. Knepper, D. Katabi, and D. Rus, "RF-compass: Robot object manipulation using RFIDs," in *Proc. 19th Annu. Int. Conf. Mobile Comput. Netw. (MobiCom)*, 2013, pp. 3–14.
- [23] D. M. Dobkin, The RF in RFID: Passive UHF RFID in Practice. Newton. MA. USA: Newnes, 2007.
- [24] Alien Technology. (2015). ALN-9640 Squiggle Inlay. [Online]. Available: http://www.alientechnology.com/tags/squiggle/
- [25] C. A. Balanis, Antenna Theory: Analysis and Design, 3rd ed. Reading, MA, USA: Addison-Wesley Longman Publishing Co., Inc, 2005.
- [26] Alien Technology. (2016). ALR-9900+. [Online]. Available: http://www.alientechnology.com/products/readers/
- [27] Impinj. (2020). R420. [Online]. Available: http://www.impinj.com
- [28] (2019). Directional Flat Panel Antenna. [Online]. Available: https://www.lairdconnect.com/rf-antennas
- [29] MathWorks. (2018). Antenna Toolbox. [Online]. Available: https://www.mathworks.com/products/antenna.html
- [30] E. Hecht, *Optics*. London, U.K.: Pearson Education, 2016.
- [31] S. M. Bowers, A. Safaripour, and A. Hajimiri, "Dynamic polarization control," *IEEE J. Solid-State Circuits*, vol. 50, no. 5, pp. 1224–1236, May 2015.
- [32] J. Hightower, R. Want, and G. Borriello, "SpotON: An indoor 3D location sensing technology based on RF signal strength," Dept. Comput. Sci. Eng., Univ. Washington, Seattle, WA, USA, Tech. Rep. 2000-02, 2000
- [33] H.-J. Lee and M. Lee, "Localization of mobile robot based on radio frequency identification devices," in *Proc. SICE-ICASE Int. Joint Conf.*, Oct. 2006, pp. 5934–5939.
- [34] J. Maneesilp, C. Wang, H. Wu, and N.-F. Tzeng, "RFID support for accurate 3D localization," *IEEE Trans. Comput.*, vol. 62, no. 7, pp. 1447–1459, Jul. 2013.
- [35] T. Wei and X. Zhang, "Gyro in the air: Tracking 3D orientation of batteryless Internet-of-Things," in *Proc. ACM MOBICOM*, 2016, pp. 55–68.
- [36] L. Shangguan and K. Jamieson, "Leveraging electromagnetic polarization in a two-antenna whiteboard in the air," in *Proc. 12th Int. Conf. Emerg. Netw. Exp. Technol.*, Dec. 2016, pp. 443–456.
- [37] R. Krigslund, P. Popovski, G. F. Pedersen, and K. Bank, "Potential of RFID systems to detect object orientation," in *Proc. IEEE Int. Conf. Commun. (ICC)*, Jun. 2011, pp. 1–5.
- [38] R. Krigslund, S. Dosen, P. Popovski, J. L. Dideriksen, G. F. Pedersen, and D. Farina, "A novel technology for motion capture using passive UHF RFID tags," *IEEE Trans. Biomed. Eng.*, vol. 60, no. 5, pp. 1453–1457, May 2013.



Jia Liu (Member, IEEE) received the B.E. degree in software engineering from Xidian University, Xi'an, China, in 2010, and the Ph.D. degree in computer science and technology from Nanjing University, Nanjing, China, in 2016. He is currently a Research Associate Professor with the Department of Computer Science and Technology, Nanjing University. His research interest includes RFID systems. He is a member of the ACM.



Shigang Chen (Fellow, IEEE) received the B.S. degree from the University of Science and Technology of China in 1993 and the M.S. and Ph.D. degrees from the University of Illinois at Urbana–Champaign in 1996 and 1999, respectively, all in computer science. He was with Cisco Systems for three years. He joined the University of Florida in 2002, where he is currently a Professor with the Department of Computer and Information Science and Engineering. He served on the Technical Advisory Board for Protego Networks Inc., from 2002 to 2003 and as

the CTO for Chance Media Inc., from 2012 to 2014. He has published more than 140 peer-reviewed journal articles/conference papers. He holds 12 U.S. patents. His research interests include computer networks, Internet security, wireless communications, and distributed computing. He received the IEEE Communications Society Best Tutorial Paper Award and the NSF CAREER Award. He served in various chair positions or as a committee member for numerous conferences. He is an Associate Editor of the IEEE/ACM TRANSACTIONS ON NETWORKING and served as an editor for a number of other journals.



Min Chen (Member, IEEE) received the B.E. degree in information security from the University of Science and Technology of China in 2011 and the M.S. and Ph.D. degrees in computer science from the University of Florida in 2015 and 2016, respectively. He is currently a Software Engineer with Google Inc. His advisor is Dr. S. Chen. His research interests include the Internet of Things, big network data, next-generation RFID systems, and network security.



Qingjun Xiao (Member, IEEE) received the B.Sc. degree from the Computer Science Department, Nanjing University of Posts and Telecommunications, China, in 2003, the M.Sc. degree from the Computer Science Department, Shanghai Jiao Tong University, China, in 2007, and the Ph.D. degree from the Computer Science Department, The Hong Kong Polytechnic University, in 2011. He joined the Computer Science Department, Georgia State University, and the Computer Science Department, University of Florida. He was a Post-

Doctoral Researcher for three years combined. He is currently an Associate Professor with Southeast University, China. He has published 16 articles as the first author on high-quality conferences or journals. His research interests include protocol and algorithm design in wireless sensor networks, RFID systems, or for network traffic measurement. He is a member of the ACM and China Computer Federation (CCF).



Lijun Chen received the B.S. degree in electrical engineering from the Xi'an University of Science and Technology, China, in 1982, and the M.S. and Ph.D. degrees in automatic control from the China University of Mining and Technology, China, in 1993 and 1998, respectively. He was a Post-Doctoral Fellow at Nanjing University, China, from 1998 to 2000, and Michigan State University, USA, from 2001 to 2002, and a Visiting Scholar at The Hong Kong Polytechnic University in 2007. His current research interests include distributed computing and quantum communications.